Current Applied Science and Technology Vol. 23 No. 1 (January-February 2023)

Research article

Energy Distribution Functions of Ions Generated by a Circular-type Anode Layer Ion Source

Nopphon Saowiang, Nitisak Pasaja and Phitsanu Poolcharuansin*

Technological Plasma Research Unit, Department of Physics, Mahasarakham University, Mahasarakham, Thailand

Received: 16 November 2021, Revised: 27 March 2022, Accepted: 6 June 2022

DOI: 10.55003/cast.2022.01.23.008

Keywords

ion energy distribution function;

retarding field energy analyzer;

anode layer ion source;

anode sheath;

cathode sheath

Abstract

An anode layer ion source, or an ALIS, is classified as a gridless ion source that produces a high-energy ion beam for either surface etching or thin film deposition. In the present work, the energy distribution functions of the ions generated in a circular ALIS were measured using a retarding field energy analyzer (RFA). Consequently, the average density and energy of the ions arriving at the ground surface were determined for the given range of process parameters. The IEDFs show two different groups of ions, namely, a narrow low energy group and a broad high energy group. The low-energy ions are probably generated in the background plasma and accelerated via the cathode sheath adjacent to the RFA. High-energy ions, on the other hand, are possibly generated in the discharge channel and gain an energy of up to $0.7eV_{anode}$ through the anode sheath. The variations in average ion energies and densities as a function of process conditions could be due to the potential profile between the source and the ground surface.

1. Introduction

An anode layer ion source (ALIS) is classified as a closed drift ion generator. The high voltage sheath adjacent to the anode effectively causes the ion generation and acceleration at a closed path of the E×B electron drift [1]. Depending on the shape of the closed path, an ALIS can produce a circular or rectangular profile on a substrate surface placed perpendicularly to the beam axis. The scalability of the ion source can enable industrial applications for large area treatment [2]. An ALIS is typically operated without the assistance of hot-filaments and grid electrodes. Thus, the system is less complex than that of conventional gridded ion sources [3]. In addition, the filament-free gridless ion source can be operated in highly reactive gases [4], e.g., N_2 and O_2. Moeover, enhanced chemical

*Corresponding author: E-mail: phitsanu.p@msu.ac.th

etching [2, 5, 6], ion-assisted surface treatment [7-9], and compound film deposition are possible using ALIS [10-13].

An ALIS, which generates high-energy ions, is typically driven by a DC positive voltage ranging from a few hundred volts to a few kV. Depending on the process parameters, the ion source can be operated in diffusion mode [14] or collimated mode [15]. In diffusion mode, the ion source is characterized by a high-current and low-voltage discharge. As a result, a relatively high ion current density can be achieved, which is applicable for ion-assisted thin film deposition [7]. In the collimated mode, in contrast, the ion source is operated under low-current high-voltage conditions. A well-defined collimated ion beam with the gained energy corresponding to anode voltage can be produced.

In thin film deposition, the ion energy significantly affects the microstructure and properties of the deposited film [16]. For example, Meškinis *et al*. [17] reported that high-sp^3 amorphous carbon films can be optimized using an ALIS ion beam with an energy of 500 eV. Excessive energy induces film damage and disorders the sp^3 structure [10]. Tian *et al*. [12] pointed out that the highest hardness of cubic boron nitride films , which is directly linked to the bombarding energy during film growth, can be achieved using an ALIS power of 200 W. Therefore, monitoring the ion energy is essential for precisely controlling ALIS-assisted thin film deposition.

Lee *et al*. [5] employed a retarding field energy analyzer, RFA, to diagnose the IEDFs of Ar and O_2 ions in the ALIS system and the IEDFs measured indicate the existence of two ion groups, namely, low-energy and high-energy ions. In addition, Park *et al*. [18] reported that the average energy of the ALIS ions, determined from the IEDFs, is proportional to the applied anode voltage and depends on the feedstock gas.

In the present work, we employed a retarding field energy analyzer to investigate the ion energy distributions for the given process conditions in more detail. The ion parameters, including average density and energy, can be determined using the measured IEDFs. Finally, a discussion on the origin of ALIS ions is provided.

2. Materials and Methods

In this work, we performed IEDF measurements of a circular-type ALIS, as shown in Figure 1. The ion source consisted of an annular discharge channel with inner and outer radii of 16 mm and 19 mm, forming a circular discharge channel with a width of 3 mm. The gap between the anode and the cathode was 1 mm. The electrode configuration of the ion source fell in the same category as linear ion sources found in the literature [4, 19]. Two concentric magnet rings adhered to the water-cooled anode provided a radial magnetic field across the discharge gap. The strength of the magnetic field at the discharge channel was approximately 0.1 T. A direct current power supply (Spellman, SL600), operating in a voltage regulation mode, was employed to energize the ion source. The power supply was able to provide positive voltages up to 3 kV; however, the maximum output was limited to 1 kV to prevent hard arcing in the ion source. The ALIS was equipped with a 15-liter vacuum chamber evacuated to a base pressure of better than 5×10^{-6} torr using a turbo molecular and a rotary vane pump. Argon was used as a process gas admitted to the vacuum chamber with flow rates up to 20 sccm, giving rise to process pressures ranging between 0.5 and 7.0 mTorr.

The energy distribution functions of the ion beam were measured using a retarding field analyzer. Details of the principle and design of the analyzer can be found in Benedikt *et al*. [20]. Here, the three-gridded RFA was employed with the grid configuration as follows. The first grid was electrically ground for plasma shielding. The second grid was biased to a programmable positive voltage source for ion retarding. Due to the limitations of the probe acquisition system

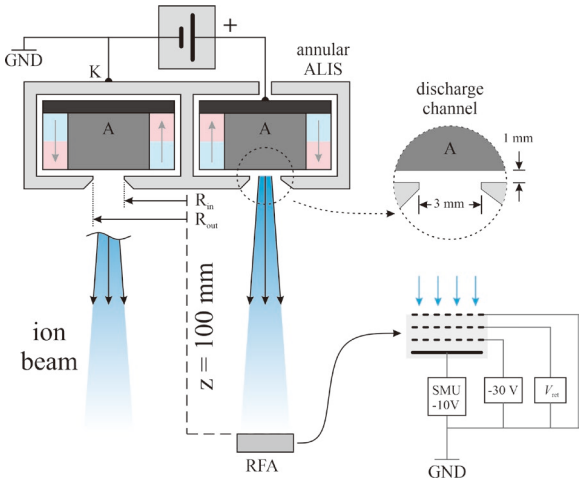

Figure 1. Schematic diagram of the experimental arrangement to measure the IEDFs of the ALIS along the radial position using three-gridded RFA

employed in this work, the retarding voltage (V_{ret}) was scanned from 65 V to 650 V, which corresponded to the energy spectrum between 65 eV and 650 eV for singly charged ions. The third grid and the collector were biased to fixed voltages of -30 V and -10 V, respectively. As a result, the potential structure in front of the collector could minimize the contribution of the secondary electrons to the collector current (I_p), which was measured using a source meter unit (SMU 2450, Keithley).

As suggested in Böhm and Perrin [21], the energy distribution function $f(V_{ret})$ of the sampling ions can be written in terms of the retarding voltage, V_{ret} as

$$f(V_{ret}) = -\frac{1}{\chi A e}\sqrt{\frac{M}{2e}}\frac{1}{\sqrt{V_{ret}}}\frac{dI_p}{dV_{ret}} \tag{1}$$

where χ is the total grid transparency, A is the accepted area, e is the fundamental charge, and M is the ion mass. Once the IEDF is known, the ion parameters in a given energy range can be obtained using the equations below.

$$\langle n_i \rangle = \int_{V_{min}}^{V_{max}} f(V_{ret})\, dV_{ret} \tag{2}$$

$$\langle \mathrm{E_i} \rangle = \frac{\int_{V_{min}}^{V_{max}} V_{ret} f(V_{ret})\, dV_{ret}}{\langle n_i \rangle} \tag{3}$$

where we assigned $\langle n_i \rangle$ as the ion density in units of m^{-3}, $\langle E_i \rangle$ as the average ion energy in units of eV, and V_{min} and V_{max} as the minimum and maximum ion retarding voltages, respectively, defining the energy range of the obtained IEDF.

3. Results and Discussion

The anode current, I_{anode}, as a function of anode voltage, V_{anode}, for the given Ar pressures is shown in Figure 2. The axes are plotted on the log scale. The discharge characteristic is highly pressure-dependent. The discharge can be ignited at a relatively low voltage, which is due to the assistance of the radial magnetic field that effectively confines the electrons along the circular discharge channel [1]. The ignition voltage tends to decrease at higher pressures; however, it still requires a minimum voltage of 300 V for ignition.

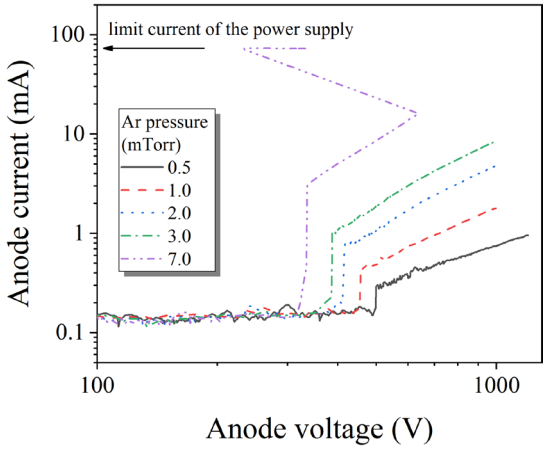

Figure 2. Discharge characteristics of the anode layer ion source plotted in log-scale of the anode current versus the anode voltage for the given argon pressures

After ignition, the discharge current can be developed further depending on the anode voltage and the operating pressure p_{Ar}. The ALIS can be driven by a high voltage up to several thousand volts raising I_{anode} to several mA ranges at relatively low pressures. Murmu *et al.* [22] operated the ALIS using V_{anode} of up to 8 kV; nevertheless, V_{anode} of less than 3 kV is typically used. The upper limit of the anode voltage in the present work was determined by arcing at the ion source, which frequently occurs when V_{anode} > 1.2 kV, particularly when operating at high pressures. The maximum V_{anode} depends on several factors, including the surface conditions of the electrodes, magnetic field strength, the process gas, and the ion source configuration. Arcing can produce noise during IEDF measurements. In addition, arcing may also generate macro-particles at the discharge gap, which can cause possible damage to the delicate grid electrodes of the RFA probe. Therefore, we operated the ALIS using an anode voltage of less than 1 kV, preventing damage to the power supply and the RFA probe.

The discharge current significantly increases with pressure. However, operating at relatively high pressure caused abruption of the anode voltage concurrent with a significant jump in the anode current. For example, at p_{Ar} = 7 mTorr, the V_{anode} drops from 630 V to 230 V, while the I_{anode} increased to the limiting current of the employed power supply.

Using the *IV* anode characteristic, Ide-Ektessabi *et al.* [19] suggested that an ALIS can be operated in two modes, namely, (i) collimated mode and (ii) diffusion mode. A low-divergence or collimating ion beam can be obtained in the former mode, while the latter produces a broader beam. The investigation performed in this work was limited to the collimated mode where beam-like energetic ions were generated.

To investigate the energy distribution of the collimated ions, RFA was employed as a diagnostic tool located at a substrate position (see Figure 1). An example of an *IV* characteristic of the RFA aligned to the discharge channel at the radial position of r ~ 15 mm is shown in Figure 3(a). The ALIS was operated using V_{anode} = 650 V at p_{Ar} = 2.4 mTorr. The probe current ranges from -80 nA to +1 nA using V_{ret} from 65 V to 650 V. The majority of the probe current is a negative current, indicating that the ion flux arriving at the collector is larger than the electron flux for most given V_{ref}. The small saturation current, i.e. +1 nA at V_{ret} > 600 V, indicates that the RFA can effectively suppress the plasma electrons from the sampling beam. Therefore, the probe current can represent the characteristics of the ion beam at the probe position. The *IV* characteristic in Figure 3(a) reveals a two-step decrease in the ion current. The first decrease is very sharp at V_{ret} ~ 130 V. A gradual decrease occurs when V_{ret} is in the range of 350 V to 450 V. The two-step decrease in the probe current may reflect the existence of two different ion groups available in the sampling beam.

The IEDF can be obtained by taking the first derivative of ion current with respect to retarding voltage, as expressed in equation (1). Considering the relevant factors, the IEDF can be plotted as a function of the retarding voltage, as depicted in Figure 3(b). Two distinguishable peaks can be observed in the IEDF. However, the portion at V_{ret} < 65 V cannot be acquired due to the limitation of the high-voltage acquisition system. The separate checks with the low-voltage acquisition confirm that the IEDF shown in Figure 3(b) is unaffected by the missing part.

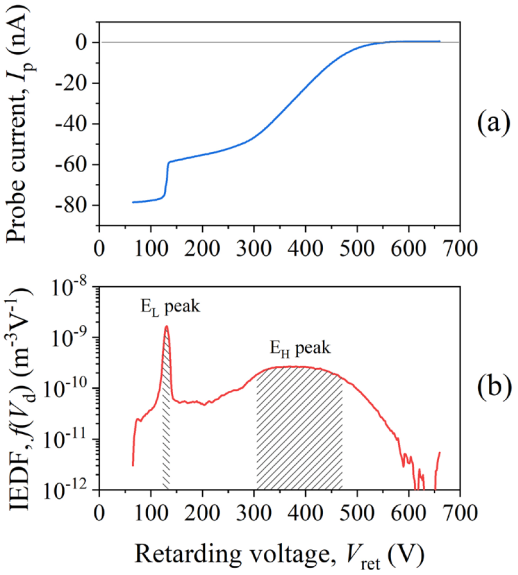

Figure 3. (a) An *IV* characteristic of the RFA and (b) the corresponding ion energy distribution function showing two distinguishable peaks, namely, a narrow low-energy (E_L) and a broad high-energy (E_H) peak. The data is obtained using V_{anode} = 650 V at p_{Ar} = 2.4 mTorr.

The obtained IEDF indicates that narrow low-energy (E_L) and broad high-energy (E_H) ions are available in the ion beam at the probe position. The low-energy peak in IEDF presents low-energy ions with the most likely energy of ~130 eV. The full width at half maximum (FWHM) of the E_L peak is ~10 eV. In contrast, the E_H peak is much broader with the FWHM of ~180 eV. The center of the E_H peak is located at ~380 eV, equivalent to the 0.58 eV_{anode}. In addition, the tail of the E_H peak is extended up to the anode voltage.

To extract the essential parameters, e.g., the average density and energy of the low- and high-energy ions, we separate the IEDF into two parts using a select V_{ret} = 150 V as the boundary between the low and high portions. Using equations (2)-(4), we can determine the ion parameters, as summarized in Table 1.

Table 1. Summary of ion parameters obtained from the IEDF in Figure 3(b)

	V_{min} (V)	V_{max} (V)	density (m^{-3})	energy (eV)
Full IEDF	65	650	$\langle n_i \rangle = 6.0\times10^{13}$	$\langle E_i \rangle = 273$
Low-energy portion	65	150	$\langle n_L \rangle = 2.2\times10^{13}$	$\langle E_L \rangle = 127$
High-energy portion	150	650	$\langle n_H \rangle = 3.8\times10^{13}$	$\langle E_H \rangle = 359$

We can see that the sampled ions at the probe position are dominated by the energetic group carrying average kinetic energy $\langle E_H \rangle$ of 359 eV, while the low-energy ions with $\langle E_L \rangle$ = 127 eV are in the minority. The analysis demonstrates that RFA can extract the quantitative details of the ions available in the ALIS system. We further report the effects of the anode voltage and the argon pressure on the ion parameters at the same probe position of r ~ 15 mm and z = 10 cm.

The anode voltage dependency of the IEDFs and the ion parameters are shown in Figure 4. The ALIS was operated at an argon pressure of 2.4 mTorr. The RFA was located at r ~15 mm aligned to the discharge channel. As seen in Figure 4(a), the anode voltage significantly affects the IEDFs. The low-energy peak seems to not alter in terms of the position but noticeably increases in magnitude. In contrast, the anode voltage extends the energy tail and widens the peak of the high-energy portion.

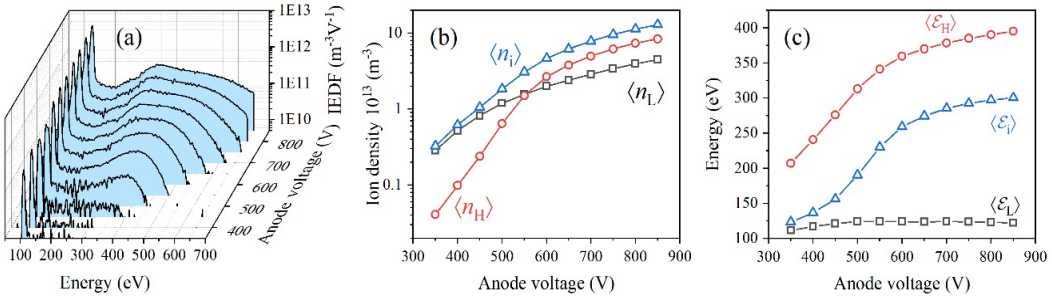

Figure 4. The anode voltage dependency of (a) the IEDFs, (b) average ion density, and (c) average ion energy at the fixed argon pressure of 2.4 mTorr and the RFA position of r ~15 mm

The IEDF analysis reveals that the increase in the anode voltage causes density and energy enhancement (see Figures 4(b) and 4(c)). The average ion density $\langle n_i \rangle$ rises over one order of magnitude, while the average ion energy $\langle E_i \rangle$ increases more than twofold. Further analysis also shows that the low-energy group dominates the sampling ions when $V_{anode} < 500$ V. The high-energy ions dominate the sampling ions when increasing the anode voltage. At a large anode voltage, e.g., $V_{anode} > 700$ V, the density of the high-energy group $\langle n_H \rangle$ is nearly double that of the low-energy group $\langle n_L \rangle$.

The average energy of the low-energy group $\langle E_L \rangle$ is almost independent of the anode voltage. The $\langle E_L \rangle$ is approximately 122 eV within a narrow deviation of 4 eV. In contrast, the high-energy ions can gain the average energy $\langle E_H \rangle$ from 200 eV up to 400 eV, relating to the energy tail

elongation observed in Figure 4(a). It is worth noting that the increasing rate of $\langle E_H \rangle$ with respect to eV_{anode} could infer the efficiency of the energy gained by the anode voltage. The rate is as high as 0.7 in the low-energy-dominated region. However, the rate dramatically decreases to ~0.1 in the high-energy dominated region.

Figure 5 presents the energy distribution functions and average parameters of the ions in the ALIS operated at V_{anode} of 650 V for the given argon pressures, p_{Ar}. It is worth noting that p_{Ar} can be determined by varying the argon flow rate at a fixed pumping speed. The IEDFs in Figure 5(a) show that both peak positions shift to lower values when operating at higher pressure. The position of the low-energy peak, for example, shifts from ~200 V at p_{Ar} = 1.0 mTorr to ~100 V at p_{Ar} = 3.0 mTorr. The position of the high-energy group may be less affected, dropping by approximately 30%, from 480 V to 330 V. However, the energy tail of the IEDFs extends to the same position of ~ 625 V. The upper limit of the IEDF tail is independent of the argon pressure. One can notice that the RFA signal and the anode current at p_{Ar} = 0.5 mTorr are significantly weak, causing unreliable IEDF. This condition is, therefore, outside the investigated range.

The average ion parameters plotted in Figure 5(b) are obtained from the entire portion of the IEDFs. The average ion density tends to increase with pressure. In contrast, the average ion energy significantly drops from 335 eV at 1 mTorr to 216 eV at 3 mTorr. It should be noted that the densities and energies of the high- and low-energy ions (not shown here) show similar trends to the average parameters. This indicates that the operating pressure affects both ion groups in the same manner.

The argon gas density is proportional to the argon pressure at a constant gas temperature. The increase in the argon gas density leads to enhancement of the ionization rate at the discharge gap, increasing the average density of the argon ions $\langle n_i \rangle$ measured at the probe position. The increase in p_{Ar} also increases the rates of collisions between the accelerated ions and the residual argon gas. As a result, the average energy on the ions $\langle E_i \rangle$ at the RFA probe tends to decrease, which agrees well with the measured IEDF and the obtained ion parameters in Figure 5.

The IEDF measurements using RFA revealed the details of the relevant parameters of the ion beam produced by the circular-type ALIS. There are two ion groups observed in the collimated mode, namely, the low-energy and high-energy ions. The investigation indicates that these ion groups show distinguishable characteristics and respond differently to the process conditions. The low-energy group is characterized by a narrow peak with an FWHM of < 25 V in IEDFs. The average energy of the low-energy group is lower than 200 eV. The high-energy group exhibits a much broader peak with the energy tail extending close to V_{anode}. Based on the evidence observed, we can discuss the origin of the ions generated by the ALIS.

Once the discharge is sustained, a possible potential profile between the anode and the probe can be sketched, as shown in Figure 6. The potential profile can be divided into three regions: (i) the anode sheath, (ii) the plasma bulk, and (iii) the cathode sheath.

The positive anode sheath is formed above the surface to collect plasma electrons and accelerate the plasma ions generated in the discharge channel [23, 24]. The maximum potential is located at the anode, forming a large potential gradient in the discharge channel [19]. The ions generated adjacent to the discharge channel experience acceleration, forming the high-energy group (E_H ions). The IEDFs indicate that most of the ions in this group are generated above the anode surface, where the local potential is a fraction of V_{anode}.

Since there is no external neutralizer in the present configuration, the plasma potential with respect to the system ground could be high to balance the ion flux generated at the anode. Chauhan *et al*. [25] reported that the plasma potential of a magnetically constricted anode is in the range of a few hundred volts. The potential in the plasma bulk causes the cathode sheath to be in front of the

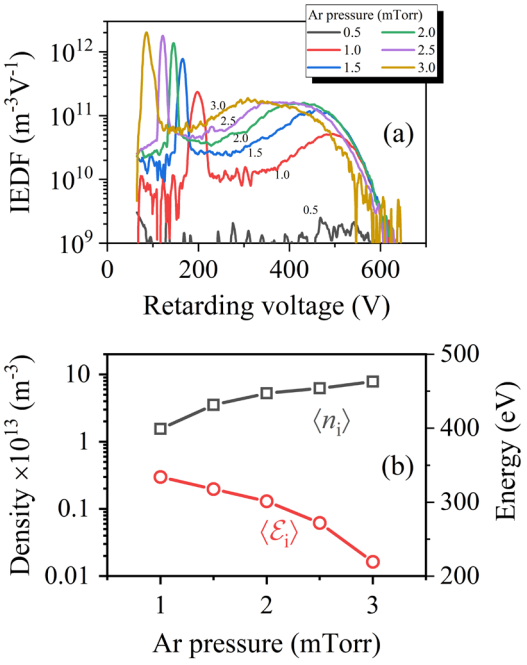

Figure 5. (a) The IEDFs and (b) the average ion parameters during the variation of argon pressure using the anode voltage of 650 V

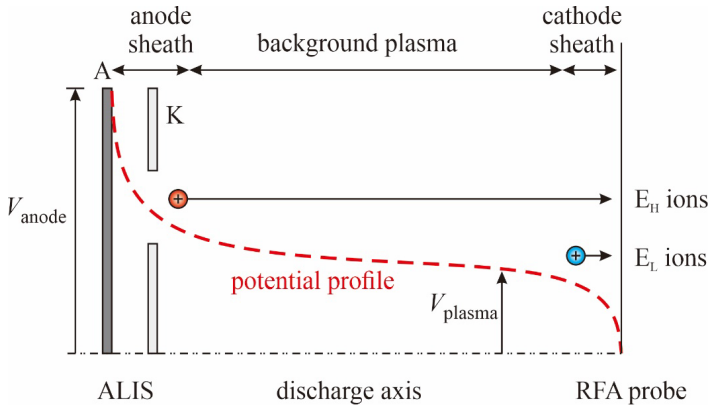

Figure 6. Sketch of possible profiles of the anode sheath at the discharge channel and the cathode sheath in front of the ground surface

ground electrode. Therefore, the ions generated in the background plasma are accelerated through the cathode sheath, forming the low-energy group (E_L ions) found in the IEDFs.

According to the discussion above, we argue that high-energy ions, E_H ions, are generated at the discharge channel, while low-energy ions, E_L ions, are produced in the background plasma.

The E_H ions are sensitive to the anode sheath. In contrast, the cathode sheath formed in front of the ground surface significantly affects the E_L ions.

The increase in V_{anode} raises the anode sheath and shifts the energy of E_H ions to a higher value. However, V_{anode} has no effect on the energy of E_L ions, which could explain the measurements in Figure 4. It is known that operating at a higher argon pressure gives rise to higher scattering and ionization frequency in the plasma bulk. The E_H ions could lose energy through scattering collisions. Lee *et al*. [26] reported that a higher operating pressure can lower the plasma potential and modify the plasma sheath profile in the RF plasma bulk. This is mainly due to the change in the electron density and temperature in the plasma [26]. In the ALIS system, the anode and cathode sheath is expected to change accordingly. Therefore, the shifts to the low energies of E_H and E_L ions, as shown in Figure 5, can possibly be attributed to the decrease in plasma potential and the modified potential profile when operating at a higher pressure.

4. Conclusions

The energy distribution functions of ions produced in a circular-type ALIS were investigated using RFA. The relevant parameters, including the average density and energy of the ions arriving at the ground surface, were obtained. The IEDFs indicate that there are two groups of ions available in the ALIS system. One is the broad high-energy group, and the other is the narrow low-energy group. High-energy ions are produced in the discharge channel, gaining up to $0.7eV_{anode}$ in the anode sheath. Low-energy ions are likely generated in the plasma bulk and move to the ground surface through the cathode sheath. The variations in the ion parameters for the process conditions could be explained by considering the potential profile between the source and the ground surface. The ion parameters obtained from the IEDF measurements could precisely control etching and deposition processes using the energetic ions in the ALIS system.

5. Acknowledgments

The authors are grateful to Mahasarakham University for financial support under Contract No. 5905016.

References

[1] Abolmasov, S.N., 2012. Physics and engineering of crossed-field discharge devices. *Plasma Sources Science and Technology*, 21(3), DOI: 10.1088/0963-0252/21/3/035006.

[2] Anders, A., 2005. Plasma and ion sources in large area coating: A review. *Surface and Coatings Technology*, 200(5-6), 1893-1906.

[3] Zhurin, V.V., 2012. *Industrial Ion Sources: Broadbeam Gridless Ion Source Technology*. Weinheim: WILEY-VCH.

[4] Dudnikov, V. and Westner, A., 2002. Ion source with closed drift anode layer plasma acceleration. *Review of Scientific Instruments*, 73(2), 729-731.

[5] Lee, S., Byun, E.-Y., Kim, J.-K. and Kim, D.-G., 2014. Ar and O-2 linear ion beam PET treatments using an anode layer ion source. *Current Applied Physics*, 14, S180-S182.

[6] Scheer, H.C., 1992. Ion sources for dry etching: Aspects of reactive ion beam etching for Si technology (invited)[a]. *Review of Scientific Instruments*, 63(5), 3050-3057, DOI: 10.1063/1.1142605.

[7] Qasim, A.M., Ali, F., Wu, H., Fu, R.K.Y., Xiao, S., Li, Y., Wu, Z. and Chu, P.K., 2019. Effects of ion flux density and energy on the composition of TiNx thin films prepared by magnetron sputtering with an anode layer ion source. *Surface and Coatings Technology*, 365, 58-64.

[8] Qasim, A.M., Ali, F., Wu, H., Fu, R.K.Y., Xiao, S., Li, Y., Wu, Z. and Chu, P.K., 2019. Enhanced mechanical and electrochemical properties of TiNx thin films prepared by magnetron sputtering with an anode layer ion source. *Surface and Coatings Technology*, 365, 253-260.

[9] Qasim, A.M., Ruan, Q., Fu, R.K.Y., Ali, F., Mehrjou, B., Wu, H., Liu, L., Wu, Z. and Chu, P.K., 2019. Enhanced oxygen-induced properties of bulk oxygenated amorphous carbon films deposited with an anode layer ion source. *Vacuum*, 169, DOI: 10.1016/j.vacuum. 2019.108915.

[10] Kahn, M., Čekada, M., Schöberl, T., Berghauser, R., Mitterer, C., Bauer, C., Waldhauser, W. and Brandstätter, E., 2009. Structural and mechanical properties of diamond-like carbon films deposited by an anode layer source. *Thin Solid Films*, 517(24), 6502-6507.

[11] Kim, W.R., Park, M.S., Jung, U.C., Kwon, A.R., Kim, Y.W., Chung, W.S., 2014. Effect of voltage on diamond-like carbon thin film using linear ion source. *Surface and Coatings Technology*, 243, 15-19.

[12] Tian, S., Xu, F., Ye, P., Wu, J., Zou, Y. and Zuo, D., 2018. Deposition of cubic boron nitride films by anode layer linear ion source assisted radio frequency magnetron sputtering. *Thin Solid Films*, 653, 13-18.

[13] Murmu, P.P., Markwitz, A., Suschke, K. and Futter, J., 2014. A novel radial anode layer ion source for inner wall pipe coating and materials modification-Hydrogenated diamond-like carbon coatings from butane gas. *Review of Scientific Instruments*, 85(8), DOI: 10.1063/1.4892813.

[14] Tang, D.L., Pu, S.H., Wang, L.S., Qiu, X.M. and Chu, P.K., 2005. Linear ion source with magnetron hollow cathode discharge. *Review of Scientific Instruments*, 76(11), DOI: 10.1063/1.2130933.

[15] Lee, S., Kim, J.-K. and Kim, D.-G., 2012. Effects of electrode geometry on the ion beam extraction of closed drift type anode layer linear ion source. *Review of Scientific Instruments*, 83(2), DOI: 10.1063/1.3665961.

[16] Anders, A., 2010. A structure zone diagram including plasma-based deposition and ion etching. *Thin Solid Films*, 518(15), 4087-4090.

[17] Meškinis, Š., Kopustinskas, V., Tamulevičienė, A., Tamulevičius, S., Niaura, G., Jankauskas, J. and Gudaitis, R., 2010. Ion beam energy effects on structure and properties of diamond like carbon films deposited by closed drift ion source. *Vacuum*, 84(9), 1133-1137.

[18] Park, D.-H., Kim, J.-H., Ermakov, Y. and Choi, W.-K., 2008. Linear ion source with closed drift and extended acceleration region. *Review of Scientific Instruments*, 79(2), DOI: 10.1063/ 1.2821507.

[19] Ide-Ektessabi, A., Yasui, N. and Okuyama, D., 2002. Characteristics of an ion beam modification system with a linear ion source. *Review of Scientific Instruments*, 73(2), 873-876.

[20] Benedikt, J., Kersten, H. and Piel, A., 2021. Foundations of measurement of electrons, ions and species fluxes toward surfaces in low-temperature plasmas. *Plasma Sources Science and Technology*, 30(3), DOI: 10.1088/1361-6595/abe4bf.

[21] Böhm, C. and Perrin, J., 1993. Retarding-field analyzer for measurements of ion energy distributions and secondary electron emission coefficients in low-pressure radio frequency discharges. *Review of Scientific Instruments*, 64(1), 31-44, DOI: 10.1063/1.1144398.

[22] Murmu, P.P., Markwitz, A., Suschke, K. and Futter, J., 2014. A novel radial anode layer ion source for inner wall pipe coating and materials modification-Hydrogenated diamond-like carbon coatings from butane gas. *Review of Scientific Instruments*, 85(8), DOI: 10.1063/1.4892813.

[23] Dorf, L., Raitses, Y. and Fisch, N.J., 2005. Experimental studies of anode sheath phenomena in a Hall thruster discharge. *Journal of Applied Physics*, 97(10), DOI: 10.1063/1.1915516.

[24] Barnat, E.V., Laity, G.R. and Baalrud, S.D., 2014. Response of the plasma to the size of an anode electrode biased near the plasma potential. *Physics of Plasmas*, 21(10), DOI: 10.1063/1.4897927.

[25] Chauhan, S., Ranjan, M., Bandyopadhyay, M. and Mukherjee, S., 2016. Droplet shaped anode double layer and electron sheath formation in magnetically constricted anode. *Physics of Plasmas*, 23(1), DOI: 10.1063/1.4939029.

[26] Lee, J.K., Babaeva, N.Y., Kim, H.C., Manuilenko, O.V. and Shon, J.W., 2004. Simulation of capacitively coupled single- and dual-frequency RF discharges. *IEEE Transactions on Plasma Science*, 32(1), 47-53, DOI: 10.1109/TPS.2004.823975.